THE JOURNAL OF BIOLOGICAL CHEMISTRY VOL. 285, NO. 39, pp. 30233–30246, September 24, 2010

Identification of a Novel Cell Death Receptor Mediating IGFBP-3-induced Anti-tumor Effects in Breast and Prostate Cancer*

Received for publication, March 11, 2010, and in revised form, March 29, 2010 Published, JBC Papers in Press, March 30, 2010, DOI 10.1074/jbc.M110.122226

Angela R. Ingermann[‡1], Yong-Feng Yang[‡1], Jinfeng Han[§], Aki Mikami[§], Amanda E. Garza[§], Lathika Mohanraj[§], Lingbo Fan[§], Michael Idowu[§], Joy L. Ware[§], Ho-Seong Kim[‡¶], Dae-Yeol Lee[‖], and Youngman Oh[‡§2]

From the [§]Department of Pathology, Medical College of Virginia Campus, Virginia Commonwealth University, Richmond, Virginia 23298-0662, the [‡]Department of Pediatrics, Oregon Health Sciences University, Portland, Oregon 97201, the [¶]Department of Pediatrics, Yongdong Severance Hospital, Yonsei University, Kangnam, Seoul 135-720, Korea, and the [‖]Department of Pediatrics, Chonbuk National University Hospital, Jeonju, Jeonbuk 560-182, Korea

Insulin-like growth factor-binding protein-3 (IGFBP-3), a major regulator of endocrine actions of IGFs, is a p53-regulated potent apoptotic factor and is significantly suppressed in a variety of cancers. Recent epidemiologic studies suggest that IGFBP-3 contributes to cancer risk protection in a variety of cancers, and a polymorphic variation of IGFBP-3 influences cancer risk, although other studies vary in their conclusions. Some antiproliferative actions of IGFBP-3 have been reported to be independent of IGFs, but the precise biochemical/molecular mechanisms of IGF-independent, antiproliferative actions of IGFBP-3 are largely unknown. Here we report a new cell death receptor, IGFBP-3R, that is a single-span membrane protein and binds specifically to IGFBP-3 but not other IGFBP species. Expression analysis of IGFBP-3 and IGFBP-3R indicates that the IGFBP-3/IGFBP-3R axis is impaired in breast and prostate cancer. We also provide evidence for anti-tumor effect of IGFBP-3R *in vivo* using prostate and breast cancer xenografts in athymic nude mice. Further *in vitro* studies demonstrate that IGFBP-3R mediates IGFBP-3-induced caspase-8-dependent apoptosis in various cancer cells. Knockdown of IGFBP-3R attenuated IGFBP-3-induced caspase activities and apoptosis, whereas overexpression of IGFBP-3R enhanced IGFBP-3 biological effects. IGFBP-3R physically interacts and activates caspase-8, and knockdown of caspase-8 expression or activity inhibited IGFBP-3/IGFBP-3R-induced apoptosis. Here, we propose that IGFBP-3R represents a novel cell death receptor and is essential for the IGFBP-3-induced apoptosis and tumor suppression. Thus, the IGFBP-3/IGFBP-3R axis may provide therapeutic and prognostic value for the treatment of cancer.

Insulin-like growth factor-binding proteins (IGFBPs)[3] are integral components of the IGF system and modulate biological actions of IGFs such as cellular proliferation, differentiation, increase in metabolic activity, and cell survival (1). Apart from its ability to inhibit or enhance IGF actions, all the IGFBPs, IGFBP-1 to -6, have been reported to exert distinct biological actions such as cell proliferation, differentiation, migration, angiogenesis, and apoptosis through an IGF/IGF-I receptor (IGF-IR)-independent manner (2–7). These intrinsic biological activities of IGFBPs appear to be critical to cardiogenesis, vascular development, and pathogenesis of cancer.

IGFBP-3, the most abundant IGFBP species in serum, circulates as a 150-kDa ternary complex with an acid-labile subunit and IGF peptide (1–3). Classically, the principal function of IGFBP-3 has been to transport IGFs, protecting them from rapid clearance and/or degradation, and modulating IGF bioavailability to cell-surface IGF receptors (8–9). Many studies have reported that IGFBP-3 exhibits distinct biological effects independent of the IGF/IGF-IR axis, in particular cell growth inhibition and induction of apoptosis in a variety of cancer cells (10–14). IGFBP-3 was shown to exert its IGF/IGF-IR-independent, antiproliferative actions via interaction with specific proteins in the extracellular, cytoplasmic and nuclear compartments of cancer cells, but the precise underlying mechanisms of IGFBP-3 have yet to be elucidated (12–16).

IGFBP-3 binding to a cell surface protein is indispensable for its antiproliferative action in human breast cancer cells, and the mid-region of IGFBP-3, which is the least conserved region among the IGFBP-1-6 protein, is responsible for cell

* This work was supported, in whole or in part, by National Institutes of Health Grant Center Core Grant 5P30NS047463 (NINDS). This work was also supported by United States Department of Defense Grants DAMD17-97-1-7204, DAMD17-02-1-0533, PC040971, and PC061151 (to Y. O.) and by the Korea Science and Engineering Foundation Grant (to D.-Y. L.).

The nucleotide sequence(s) reported in this paper has been submitted to the GenBank™/EBI Data Bank with accession number(s) FJ748884.

[1] Both authors contributed equally to this work.

[2] To whom correspondence should be addressed: 1101 East Marshall St., P. O. Box 980662, Richmond, VA 23298-0662. Tel.: 804-827-1324; Fax: 804-828-9749; E-mail: yoh@mcvh-vcu.edu.

[3] The abbreviations used are: IGFBP, insulin-like growth factor (IGF)-binding protein; IGFBP-3R, IGFBP-3 receptor; IGF-IR, IGF-I receptor; Ad, adenovirus; DD, death domain; EGFP, enhanced green fluorescent protein; FADD, Fas-associated protein with death domain; GST, glutathione *S*-transferase; HRP, horseradish peroxidase; MTT, 3-(4,5-dimethylthiazol-2-yl)-2,5-diphenyltetrazolium bromide, a tetrazolium bromide; m.o.i., multiplicity of infection; TNT, transcription and translation technique; z-DEVD-fmk, *N*-benzyloxycarbonyl-Asp-Glu-Val-Asp-fluoromethyl ketone; z-IETD-fmk, *N*-benzyloxycarbonyl-Ile-Glu-Thr-Asp-fluoromethyl ketone; z-VAD-fmk, *N*-benzyloxycarbonyl-Val-Ala-Asp-fluoromethyl ketone; RXR, retinoid X receptor; RAR, retinoic acid receptor; FBS, fetal bovine serum; PBC, phosphate-buffered saline; BSA, bovine serum albumin; RT, reverse transcriptase; ELISA, enzyme-linked immunosorbent assay; CHAPS, 3-[(3-cholamidopropyl)dimethylammonio]-1-propanesulfonic acid; shRNA, short hairpin RNA.

surface binding (17, 18). Moreover, IGFBP-3-induced apoptosis through the activation of specific caspases that are involved in the death receptor-mediated apoptotic pathways in breast cancer cells (19). These findings strongly suggest the existence of an IGFBP-3-specific receptor participating in the direct proapoptotic effect of IGFBP-3 in cancer cells.

We describe herein the cloning and characterization of a novel cDNA encoding a new cell death receptor for IGFBP-3, IGFBP-3R. We found that IGFBP-3R is a *bona fide* IGFBP-3 receptor; IGFBP-3R is expressed on the cell surface, interacts specifically with IGFBP-3, activates initiator caspase-8, and mediates IGFBP-3-induced apoptosis *in vitro* and tumor suppression *in vivo*.

EXPERIMENTAL PROCEDURES

Cell Culture—All cell lines, except M12 and the MCF-7:IGFBP-3 stable lines, were purchased from ATCC. We cultured breast cancer cells in Dulbecco's modified Eagle's medium/high glucose with 10% fetal bovine serum (FBS), PC-3 in F-12 with 10% FBS, and M12 cells in RPMI 1640 medium supplemented with 10 ng/ml epidermal growth factor, 0.02 mM dexamethasone, 5 μg/ml insulin, 5 μg/ml transferring, 5 μg/ml selenium and gentamicin at 37 °C under 5% CO_2. MCF-7:IGFBP-3 stable lines were generated from wild type MCF-7 cells using the ecdysone-inducible expression system (Invitrogen). IGFBP-3 protein production was induced with the addition of ponasterone A (Invitrogen) to the culture medium.

Proteins and Antibodies—We purchased recombinant IGF-I and IGFBP-1, -2, -4, -5, -6 from R&D Systems and AUSTRAL Biologicals. We used anti-FLAG M2, GFP, β-galactosidase, α-tubulin antibodies (Sigma-Aldrich), anti-caspase-3, caspase-8, Fas-associated death domain protein (FADD), poly(ADP-ribose) polymerase (PARP) antibodies (Cell Signaling Technologies), anti-CD34, histone deacetylases antibodies (Santa Cruz Biotechnology), HRP-conjugated secondary antibodies (Amersham Pharmacia), and fluorescently conjugated secondary antibodies (Southern Biotechnology Associates and Molecular Probes). Immunofluorescence-stained cells were visualized with Alexa 488 or fluorescein isothiocyanate (Molecular Probes).

Plasmids and Recombinant Proteins—pEGFP:IGFBP-3R was generated by subcloning the IGFBP-3R cDNA into pEGFP-N3 (Clontech). GST::IGFBP-3R protein was generated by subcloning the IGFBP-3R cDNA into the pGEX-4T-1 vector (Amersham Biosciences) in-frame with GST, transforming into *E. coli* strain BL21(DE3)pLysS, and inducing expression with isopropyl 1-thio-β-D-galactopyranoside. Gel-purified protein from cell lysates was injected into rabbits for polyclonal IGFBP-3R antibody production.

Yeast Two-hybrid Screening—An Hs578T cDNA library in pGAD10 was generated using the Two-Hybrid cDNA Library Construction kit (Clontech). The bait plasmid was constructed by amplifying an internal sequence of the IGFBP-3 cDNA (encoding amino acids 88–148) by PCR, then cloning this fragment into the pBTM116 vector, in-frame with the LexA DNA binding domain coding sequence. The bait plasmid was then transformed into yeast strain L40. A single transformant colony was selected for successive transformation with the pGAD10:Hs578T cDNA library. 663 transformant colonies that grew on selective media were replica-plated onto duplicate fresh plates, one of which was used for a β-galactosidase assay. Positive colonies were then cultured on non-selective media until the bait plasmid was lost and further tested in mating assays with the original bait strain and a false-positive screening strain expressing the pBTM116:lamin plasmid. Three colonies tested positive with the IGFBP-3 bait and negative with lamin. Plasmid DNA was isolated from these and transformed into *E. coli* TG1.

Cell Monolayer Binding Assay—Breast cancer cells were seeded into 24-well plates and grown to 60–70% confluency then transfected according to manufacturer's instructions in serum-containing medium for 36 h. Sf9 cells were seeded into 24-well plates and infected with virus harboring the IGFBP-$3R^{FLAG}$ cDNA for 48 h. Cells were washed with cold PBS, then incubated for 3 h at 12 °C in binding buffer (1× Hanks' buffered salt solution, 1 mM $CaCl_2$, 1 mM $MgCl_2$, 0.5% BSA) containing ^{125}I-IGFBP-3 (Diagnostic Systems Laboratories) at 50,000 cpm per well in triplicate with or without unlabeled IGFBP-3 as indicated in the Fig. 1 legend. The binding solution was then aspirated, and the cells were washed in cold binding buffer (without BSA), lysed in 0.25 N NaOH, and then the radiolabeled IGFBP-3 was detected in a gamma counter.

Synthesis of siIGFBP-3R—Double-stranded RNAs targeting IGFBP-3R were purchased from Dharmacon, Inc. We used 4 sets of IGFBP-3R siRNAs consisting of a 21-nucleotide sense and antisense strand: IGFBP-3R siRNA #1 (sense, 5′-GUGAGGAAUGUGUUAGUGUUU-3′; antisense, 5′-ACACUAACACAUUCCUCACUU-3′); IGFBP-3R siRNA #2 (sense, 5′-GACAACUGGUCCUUAUCACUU-3′; (antisense, 5′-GUGAUAAGGACCAGUUGUCUU-3′); IGFBP-3R siRNA #3 (sense, 5′-GGAACAAGACCCGGACAUUUU-3′, antisense 5′-AAUGUCCGGGUCUUGUUCCUU-3′); IGFBP-3R siRNA #4 (sense, 5′-GGAACCUGCCUAUAUUUUAUU-3′; antisense, 5′-UAAAAUAUAGGCAGGUUCCUU-3′). siCONTROL Non-Targeting siRNA #1 (Dharmacon) was used as a nonspecific control. A mixture of 4 sets of IGFBP-3R siRNAs (total 20 nM) was transfected for 6 days in M12 prostate cancer cells. Two target sequences corresponding to siRNAs #1 and #3 were further selected to construct shRNA plasmids using pSUPER RNAi System™ (OligoEngine): for pSRN IGFBP-3R shRNA #1 (+526 to +544; sense, 5′-gatccccGTGAGGAATGTGTTAGTGTttcaagagaACACTAACACATTCCTCACttttta-3′; antisense, 5′-agcttaaaaaGTGAGGAATGTGTTAGTGTtctcttgaaACACTAACACATTCCTCACggg-3′); for pSRN IGFBP-3R shRNA #3 (+300 to +318; sense, 5′-gatccccGGAACAAGACCCGGACATTttcaagagaAATGTCCGGGTCTTGTTCCttttta-3′; antisense, 5′-agcttaaaaaGGAACAAGACCCGGACATTtctcttgaaAATGTCCGGGTCTTGTTCCggg-3′). The complementary sequences was annealed together and inserted into the BamHI and HindIII site of pSRN, generating pSRN-IGFBP-3R shRNA #1 or pSRN-IGFBP-3R shRNA #3, respectively.

Generation of Adenoviral IGFBP-3 and IGFBP-3R—We used NotI-XbaI restriction fragments from pcDNA3/wild type IGFBP-3 cDNA and EcoR1-Xho1 restriction fragments from CS2-$IGFBP\text{-}3R^F$ to ligate into NotI-XbaI-digested pShuttle-

CMV and EcoRV-digested pShuttle-CMV, respectively. We used SalI-NotI restriction fragments from pcDNA3.1/LacZ (Invitrogen) to ligate into SalI-NotI-digested pShuttle-CMV. Recombination into the pAdEasy viral backbone was accomplished in *E. coli* strain BJ5183 according to the manufacturer's instructions. The recombination was verified, and the adenoviral recombinant DNA was transferred to DH5α. We purified recombinant pAdEasy plasmids containing CMV-cDNA inserts using Qiagen columns (Qiagen) and transfected QBI-293A cells with 5 μg of PacI-digested DNA using the calcium phosphate method (Promega). Cells were seeded at 2×10^6 cells per 150-mm culture dish 24 h before transfection. Lysis of transfected cells, indicating adenoviral growth, occurred within 4 days. After amplification, lysates containing clonal recombinant Ad were prepared from 150-mm culture dishes and purified by CsCl gradient centrifugation. Recovered virus was separated into aliquots and stored at −20 °C in 5 mM Tris, pH 8.0, buffer containing 50 mM NaCl, 0.05% bovine serum albumin (BSA), and 25% glycerol. We performed viral titrate assay using serial dilution infection of QBI-293A cells and counting plaques under an overlay of 0.3% agarose, 10% FBS, and 1× Dulbecco's modified Eagle's medium.

Semiquantitative PCR—One μg of purified total RNA was used for RT-PCR analysis using the ThermoScript RT-PCR system (Invitrogen). The sequences of the forward and reverse primers were as follows: IGFBP-3 (forward, 5′-GACTCTGCTGGTGCTGCTC-3′; reverse, 5′-GCATGCCCTTTCTTGATGAT-3′); IGFBP-3R forward (5′-ATGGGACAGTCACAGGGAAG-3′; reverse, 5′-AAGGCCACAGAAGAGAAGCA-3′); β_2M forward (5′-GTGCTCGCGCTACTCTCTCT-3′; reverse, 5′-CGGCAGGCATACTCATCTTT-3′). The IGFBP-3 PCR product is 501 bp in length, IGFBP-3R is 437 bp, and β_2M is 278 bp. For PCR amplification, 35 cycles were performed for IGFBP-3 and IGFBP-3R, and 30 cycles for β_2M (denaturation: 95 °C, 1 min; annealing: 60 °C, 1 min; polymerization: 72 °C, 1 min). Amplified products were electrophoresed on a 2.0% agarose gel, and DNA was visualized by ethidium bromide staining.

Northern Blotting—We used Human Multi-tissue Northern Blots I & II (Clontech). Total RNAs from monolayer cultures of human breast and prostate cells were harvested using the RNeasy RNA isolation kit (Qiagen). Five μg of total RNA from each cell line were run on 1% formaldehyde gels and transferred onto GeneScreen Plus nylon membranes (PerkinElmer Life Sciences). Membranes were UV-cross-linked and stained in 0.02% methylene blue, 0.3 M NaOAc, pH 5.5. ^{32}P-Labeled cDNA probes were prepared using the Prime IT II kit (Stratagene). Membranes were hybridized in Rapid-Hyb buffer (Amersham Biosciences), washed in 0.3× SSC (1× SSC = 0.15 M NaCl and 0.015 M sodium citrate), and exposed to film.

Cell Proliferation Assays—We carried out cell proliferation assays using the MTT Cell Proliferation Assay (ATCC). Cells were seeded in triplicate in 96-well microtiter plates, grown to 60–70% confluency, and treated as indicated. MTT was added to the cell culture and incubated for 4 h at 37 °C. The assays were performed according to the manufacture's protocol.

Biotinylation of IGFBP-3—Non-glycosylated *E. coli*-derived IGFBP-3 was biotinylated using the *p*-biotinoyl aminocaproic acid-*N*-hydroxy-succinamide ester (Thermo Scientific Pierce) at room temperature (20). At the end of incubation free biotin ester was separated on a Sephadex G-25 column (Bio-Rad).

In Vitro Transcription and Translation Techniques (TNT)—Each linear plasmid DNA template of IGFBP-3R and caspase-8 was translated separately in the presence of wheat germ extracts, T7b RNA polymerase, and amino acid mixture according to the manufacturer's protocol (Promega). A mixture of the two proteins was co-immunoprecipitated with IGFBP-3R antibodies, and the resultants were further Western-blotted using caspase-8 and IGFBP-3R antibodies.

IGFBP-3R Binding Assay—Cos-7 cells were infected with Ad:IGFBP-3R for 2 days. The cells were lysed in HBSST (HBSS with 0.035% sodium bicarbonate, 0.5% Triton X-100, 1 mM $MgSO_4$, and 1 mM $CaCl_2$, pH 7.4) supplemented with Halt^{TM} Protease Inhibitor (Roche Applied Sciences). A 96-well plate was coated with 50 μl of anti-FLAG antibody diluted in PBS at 10 ng/μl per well overnight at 4 °C. The wells were blocked with 300 μl of HBSST containing 5% BSA (HBSST-BSA) for 1 h at room temperature. The wells were washed 3 times with 300 μl of PBS containing 0.2% Tween 20. Cell lysates (10 μg/50 μl/well) were added and incubated for 1 h at room temperature. After washing, 16 nM biotinylated IGFBP-3 was incubated in the presence of 0–100 nM IGFBP-3 (Celtrix) for 1 h at room temperature. The wells were incubated with HRP-conjugated streptavidin (Thermo Scientific) diluted in 50 μl of HBSST-BSA for 1 h at room temperature and further incubated with 50 μl of 3,3′,5-5′-tetramethyl benzidine substrate (Sigma). The reaction was terminated by adding 50 μl of 1 N H_2SO_4, and absorbance was measured at 450 nm.

Immunofluorescence Staining—We seeded cells in a chamber slide (Lab-Tek II Chamber Slide System, Nalge Nunc International) and infected cells with Ad:IGFBP-3R for 2 days. Adherent cells were washed with PBS and fixed in 3% paraformaldehyde for 10 min at room temperature. After washing twice with PBS, cells were permeabilized with 0.1% Triton X-100 in PBS for 5 min at room temperature, washed twice with PBS, and blocked in 1% BSA with 1% normal goat serum in PBS for 30 min at room temperature. We incubated slides with α-IGFBP-3R or α-FLAG antibodies at a 1:100 dilution in blocking buffer for 30 min at room temperature and washed slides twice with PBS. We incubated slides with secondary goat anti-rabbit IgG Alexa Fluor 568 or goat anti-mouse IgG fluorescein isothiocyanate at a 1:200 dilution for 45 min followed by 3 washes with PBS. Next we counterstained the nuclei with Hoechst (1 μg/ml) for 5 min. Slides were washed three times with PBS, and stained slides were mounted with VECTASHIELD Mounting Medium (Vector Laboratories) and analyzed under a confocal microscope (Leica TCS-SP2 AOBS).

Cell Lysates, Subcellular Fraction Preparations—Cell lysates were harvested by washing monolayer cultures in ice-cold PBS then lysing in Triton lysis buffer (20 mM Tris, pH 7.6, 150 mM NaCl, 1% Triton X-100). Plates were rocked at 4 °C for 15 min, and lysates were collected and centrifuged to remove cellular debris. For subcellular fraction preparations, plasma membrane and cytosolic and nuclear fractions were isolated by homogenizing cells using the membrane protein extraction kit (Bio Vision) and centrifuging successively at 700 and 100,000 × *g* for 10 and 60 min, respectively. All pellets were solubilized in

50 mM HEPES, pH 7.4, 150 mM NaCl, 2 mM $MgSO_4$, 1% Triton X-100. Equal amounts of protein from each fraction were analyzed by SDS-PAGE followed by Western blotting for fractionation specific markers.

Immunoprecipitations and Western Blotting—For immunoprecipitations, cleared cell lysates were diluted in 20 mM Tris, pH 7.6, 150 mM NaCl and adjusted to a final concentration of 0.5% Triton X-100 (immunoprecipitation buffer). Antibodies and Protein A or Protein G-Sepharose (Amersham Biosciences) were added, and reactions were incubated at 4 °C for 4 h. Beads were washed twice in immunoprecipitation buffer and suspended in 1× reducing sample buffer. Samples were run on 12.5% reducing SDS-PAGE and electrotransferred onto Hybond-ECL nitrocellulose (Amersham Biosciences). Membranes were blocked in 5% nonfat milk, Tris-buffered saline, 0.1% Tween 20 (TBS-T). Primary antibodies were diluted in blocking solution and incubated on the membranes for 2 h at room temperature. Membranes were washed in TBS-T then incubated with HRP-conjugated secondary antibody, diluted 1:3000 for 1 h at room temperature, washed, and detected using the Renaissance Western blot Chemiluminescence reagents (PerkinElmer Life Sciences).

Caspase Inhibitor Treatment—We purchased cell-permeable caspase inhibitors from BD Biosciences. We infected MDA231 cells with Ad:IGFBP-3R or Ad:EV and further treated with 50 μM z-VAD-fmk (pan caspase inhibitor), z-IETD-fmk (caspase-8 specific inhibitor), or z-FA-fmk (inactive caspase inhibitor) every 24 h. We performed caspase-3/-7 activity assay and cell death detection ELISA assay at 48 and 72 h after infection.

Thymidine Incorporation Assay—Cells were seeded in triplicate into 24-well plates, grown to 60–70% confluency, and transfected and treated as indicated in the Fig. 4 legend. At 48 h post-transfection, the medium was replaced with serum-free medium, and cells were further incubated for 24 h. To each well 0.1 μCi of [^{3}H]thymidine was added, and the acid-precipitable radioactivity in each well was assayed 24 h later.

Caspase-3/-7 and -8 Activity Assays—Cells were subsequently cultured in media with 1% FBS and infected with Ad:IGFBP-3 or Ad:EV for 2 days, and cell lysates were prepared using CHAPS lysis buffer (50 mM HEPES, pH 7.4, 0.10% CHAPS, 0.10% Triton X-100, 0.1 mM EDTA, and 1 mM dithiothreitol) and 12,000 × *g* centrifugation at 4 °C. Caspase-3/-7 and -8 activity was measured using 10 μl of cell lysates and 10 μl of 100 μM caspase-3 and -7 substrate (Ac-DEVD-amidomethylcoumarin (AMC)) or caspase-8 substrate (Ac-IETD-AMC) in assay buffer (50 mM HEPES, pH 7.4, 100 mM NaCl, 10% CHAPS, 10% glycerol, 10 mM EDTA, and 5 mM dithiothreitol). The reaction was measured at 37 °C for 6 h, and fluorescence was measured in a fluorescence plate reader (BMG LABTECH).

Cell Death ELISA Assay—Apoptotic cell death was measured using the cell death detection ELISA (Roche Applied Sciences) according to the manufacturer's instructions. Equivalent cell populations were measured, and absorbance was measured at 405 nm (reference wavelength, 490 nm).

Intratumoral Delivery of Ad:IGFBP-3R in Vivo—Mouse experiments were performed under a protocol approved by the Virginia Commonwealth University Institutional Animal Care and Use Committee (IACUC). M12 prostate cancer cells or MDA231 breast cancer cells suspended in 100 μl of sterile PBS were injected into the dorsal flank of 4-week-old male or female athymic nude mice, respectively. Once tumor volume reached ~75 mm^3, mice were injected intratumorally 2 times at day 0 and day 6 with 5×10^9 plaque-forming units of Ad:IGFBP-3R or Ad:Lac-Z in 50 μl of PBS or 50 μl of PBS alone as a control. Tumor size and volume were measured every 2 days. We harvested tumor tissues for immunohistochemistry of β-galactosidase, IGFBP-3R, and CD34 16 days after first injection.

Human Samples—Breast and prostate tumor paraffin blocks were obtained from the archives of the Division of Surgical Pathology with approval from the Institutional Review Board of Virginia Commonwealth University. To perform semiquantitative RT-PCR, we obtained frozen-fresh prostate tumor tissues from the Tissue/Tumor Procurement Facility of the Oregon Cancer Center with approval from the Institutional Review Board of Oregon Health Sciences University. Total RNA was purified from tumor tissues using the TRIZOL (Invitrogen) extraction technique as recommended by the manufacturer. One μg of purified total RNA was used for RT-PCR analysis using the ThermoScript RT-PCR System (Invitrogen) and specific primers.

Immunohistochemistry of Human and Mouse Tissue—Slides with the human and mouse tissue sections were dried in a 65 °C oven for 1 h before staining. The tissue sections were deparaffinized in xylene and rehydrated in decreasing grades of alcohol (100, 90, and 80%) and rinsed in PBS. We quenched endogenous peroxidase activity by incubating tissue sections in 3% hydrogen peroxide for 5 min. The slides are placed in the steamer for heat target antigen retrieval at the optimal determined pH of 9. We incubated slides with the primary antibodies for IGFBP-3 (1:100 dilution), IGFBP-3R (1:100 dilution), or CD34 (1:100 dilution) for 1 h at room temperature and then rinsed twice in Dako wash buffer. We further incubated slides with appropriate secondary antibody for 30 min then rinsed and applied a HRP-labeled Envision+™ polymer. The specific antibody and conjugated polymer enzyme complex was visualized using the Envision+™ Dual Link System-HRP (DAB+) system after thorough washing. We counterstained tissue sections with Gill's III hematoxylin for 30 s.

Statistical Analyses—We conducted statistical analysis by analysis of variance with Student's *t* test. We considered a *p* value of 0.05 or less as significantly different.

RESULTS

Identification of a Novel IGFBP-3R and Its Endogenous Expression on Cell Membrane—The yeast two-hybrid screening was performed to identify a potential IGFBP-3 receptor using a cDNA construct encoding the mid region (amino acids 88–148) of the IGFBP-3 protein as bait against an Hs578T, human breast cancer cell cDNA library. This screen resulted in the identification of a cDNA, later designated IGFBP-3R, representing a novel gene composed of 915 base pairs and encoding a 240-amino acid polypeptide (GenBank™ accession

#FJ748884). Genomic data base analysis identified 4 exons composing the cDNA sequence on chromosome 16q13.

Northern blot analysis indicated a wide distribution of IGFBP-3R mRNA in human tissues. The 0.9-kb mRNA was detected to varying degrees in normal human tissues (Fig. 1*A*). A second roughly 2-kb transcript was detected in testis, the significance of which, if any, is not known. The deduced amino acid sequence indicates that IGFBP-3R consists of an N-terminal putative signal peptide sequence, three potential *N*-glycosylation sites, a putative single-span transmembrane domain, and a short C-terminal cytoplasmic domain (Fig. 1*B*). Interestingly, its transmembrane domain contains a leucine zipper-like heptad repeat pattern of amino acids similar to the single-span transmembrane leucine zipper sequences identified in erythropoietin receptor and discoidin domain receptor (Fig. 1*B*, *inset*, and Refs. 21 and 22).

To examine the endogenous protein, a rabbit polyclonal antibody was generated against GST-fused IGFBP-3R purified from *E. coli*. The IGFBP-3R antibody recognized a species of roughly 32 kDa from human breast cancer cell lysates (Fig. 1*B*, *right panel*). We further examined whether IGFBP-3R is a cell membrane protein and whether IGFBP-3 interacts with IGFBP-3R on the cell surface using monolayer binding assays with ^{125}I-labeled IGFBP-3, cell fractionation preparations by differential centrifugation, and confocal microscopy. Overexpression of IGFBP-3R resulted in a 1.5- and 3.5-fold increase in IGFBP-3 cell surface binding to MCF-7 and Sf9 cell monolayers relative to cells expressing endogenous levels of IGFBP-3R, respectively (Fig. 1*C*, *left panel*). Total binding was competed in a dose-dependent manner with the addition of unlabeled IGFBP-3, demonstrating IGFBP-3R specificity for binding IGFBP-3. The presence of the FLAG tag at the C terminus of the IGFBP-3R protein had no effect on IGFBP-3 binding (Fig. 1*C*, *right panel*). In addition, the IGFBP-3R antibody recognized a species of roughly 32 kDa in plasma membrane and cytoplasmic fractions but not in nuclear fraction in human breast cancer cells (Fig. 1*D*). In accordance with these findings, confocal microscopy confirms that both endogenously produced and overexpressed IGFBP-3R exists on the cell membrane of human breast cancer cells (Fig. 1*D*).

Specific Interaction of IGFBP-3R with IGFBP-3—To characterize the specific interaction between IGFBP-3 and IGFBP-3R in a mammalian system, coimmunoprecipitation and IGFBP-3R binding assays were performed. A coimmunoprecipitation experiment was initially carried out using the EGFP:IGFBP-3R fusion protein and FLAG-tagged IGFBP-3 produced in a baculovirus system. A specific interaction of IGFBP-3 and IGFBP-3R was observed (Fig. 2*A*). Similar results were obtained using MDA231 cells infected with adenoviral constructs containing the FLAG-tagged IGFBP-3R cDNA sequence. When cell lysates from Ad:EV- or Ad:IGFBP-3R^F-infected cells were immunoprecipitated with FLAG M2 antibodies and proteins were detected on Western immunoblots with IGFBP-3R antibodies. Both endogenous IGFBP-3R and overexpressed IGFBP-3R^F were detected in both cell lysates, whereas FLAG-tagged IGFBP-3R was detected in cell lysates from Ad:IGFBP-3R^F-infected cells after immunoprecipitation with FLAG M2 antibodies (Fig. 2*B*). When the FLAG antibody was used for immunoprecipitation, recombinant IGFBP-3 was precipitated with IGFBP-3R^F (Fig. 2, *C* and *D*). Specificity of coimmunoprecipitation was demonstrated by showing that IGFBP-3 is only coprecipitated with the Ad:IGFBP-3R^F-infected cell lysates but not with the Ad:EV-infected cell lysates (Fig. 2*D*). To further demonstrate the interaction between endogenously expressed IGFBP-3 and IGFBP-3R, MDA231-conditioned media was immunoprecipitated with IGFBP-3R antibodies in the presence/absence of MCF-7 cell lysates. As shown in Fig. 2*E*, endogenous IGFBP-3 in MDA231-conditioned media was coprecipitated with endogenously produced IGFBP-3R in MCF-7 cells when IGFBP-3R antibodies were used for immunoprecipitation. Additional coimmunoprecipitation assays with IGFBPs 1–6 reveal that the interaction of IGFBP-3 and IGFBP-3R was evident, but no interaction was detected with other IGFBPs (Fig. 2*F*). Furthermore, the IGF-I and IGFBP-3 complex was unable to bind IGFBP-3R, indicating that binding of IGFBP-3 to IGF and IGFBP-3R is mutually exclusive (Fig. 2*D*), and IGF-I may regulate the IGFBP-3/IGFBP-3R-induced biological function by preventing IGFBP-3 binding to IGFBP-3R (10). *In vitro* IGFBP-3R binding assays were further performed using biotin-labeled IGFBP-3 and purified IGFBP-3R. The interaction between IGFBP-3 and IGFBP-3R was specific and saturable (Fig. 2*G*, *left panel*). A competitive binding assay revealed a dose-dependent competition with unlabeled IGFBP-3 with $IC_{50} = 0.5$ nM but not with unlabeled IGFBP-5 (Fig. 2*G*, *right panel*).

Significance of IGFBP-3/IGFBP-3R in Human Cancer—To assess the significance of the IGFBP-3/IGFBP-3R axis in tumorigenesis, the distribution of IGFBP-3 and IGFBP-3R was examined in normal and malignant human breast and prostate specimens. Although IGFBP-3 and IGFBP-3R were readily detected in benign breast lobule and benign prostate tissues, heterogeneous but significantly reduced expression of IGFBP-3 and IGFBP-3R was observed in invasive breast ductal carcinoma and prostate adenocarcinoma cells (Fig. 3*A*). Heterogeneous but significantly reduced mRNA expression of IGFBP-3 and IGFBP-3R were also observed in prostate tissue (Fig. 3*B*). These data indicate that the IGFBP-3/IGFBP-3R axis is impaired during the progression of breast and prostate tumor, and restoration of the IGFBP-3/IGFBP-3R axis might play a role in suppression of tumor growth.

The role of IGFBP-3R in prostate and breast tumor *in vivo* was further examined with an athymic nude mouse model using M12 human prostate cancer cells and MDA231 breast cancer cells. Initial tests revealed that the adenoviral titer, 5×10^9 plaque-forming units, was optimal in terms of *in vivo* expression efficiency and cytotoxic effect on M12 prostate tumor in the nude mice (Fig. 3*C*). Intratumoral injection of Ad:IGFBP-3R^F into M12 cell tumors in nude mice resulted in a significant shrinkage of tumor mass without any obvious toxic effect on mice 16 days after viral injection. Compared with Ad:Lac-Z-infected tumor, Ad:IGFBP-3R tumor showed a 40% reduction in tumor mass (Fig. 3*D*). A similar anti-tumor effect of IGFBP-3R was obtained in a MDA231 breast tumor nude mouse model (43% reduction in tumor mass). Immunohistochemistry with CD34 antibody revealed that IGFBP-3R-overexpressed tumor also exhibit significant suppression

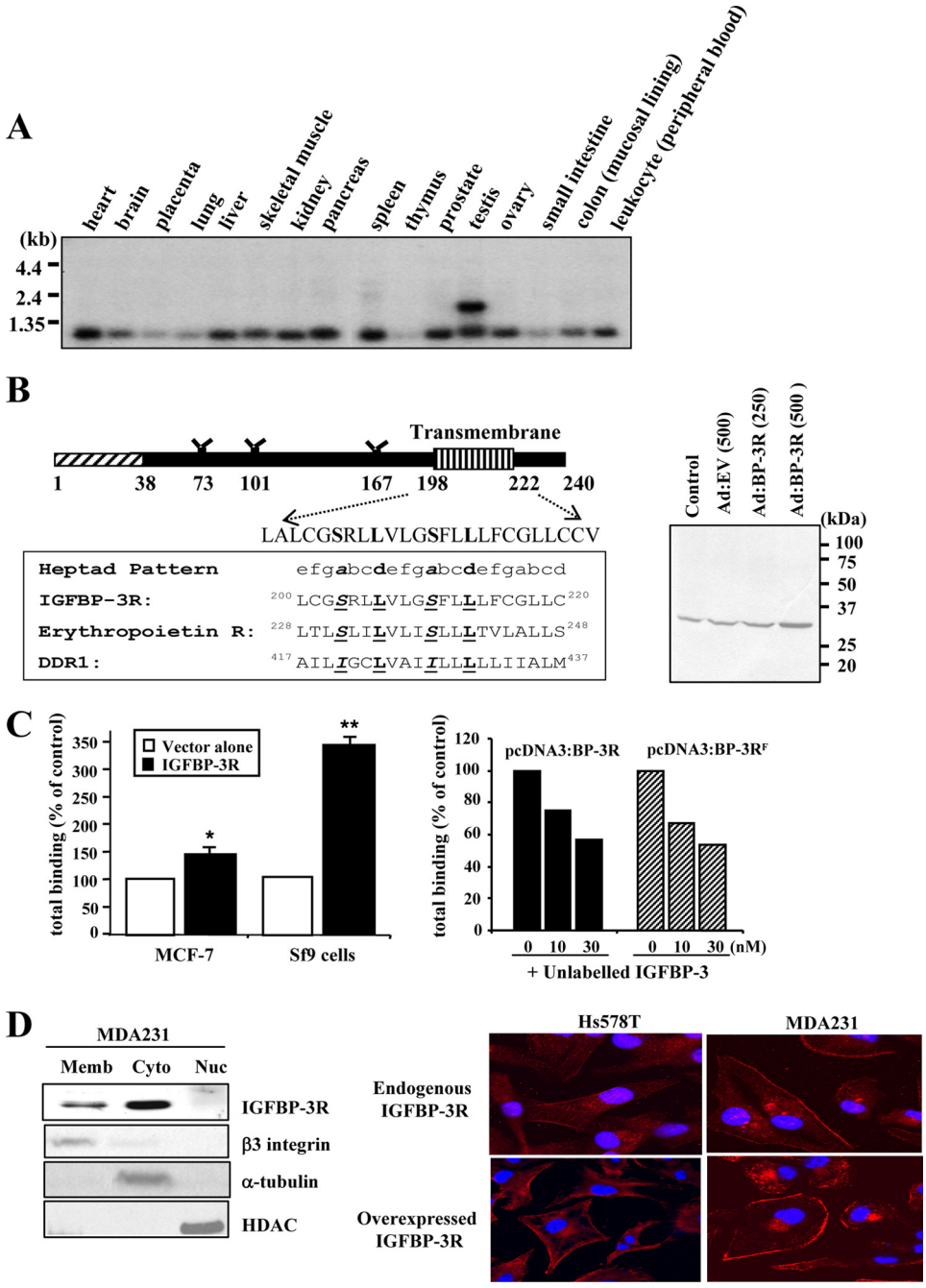

FIGURE 1. **IGFBP-3-interacting protein, IGFBP-3R, is a single-span membrane protein and widely expressed in human normal tissue but suppressed in prostate and breast tumor.** *A*, Northern blot analysis of IGFBP-3R mRNA expression is shown. Multiple human tissue Northern blots I and II (Clontech) were probed with ^{32}P-labeled IGFBP-3R cDNA. *B*, *left panel*, shown is a schematic diagram of IGFBP-3R sequences demonstrating an N-terminal putative signal peptide sequence, three potential *N*-glycosylation sites, a putative single-span transmembrane domain with a leucine zipper-like heptad repeat sequence, and a short C-terminal cytoplasmic domain. *Inset*, shown is the alignment of the putative transmembrane segment in IGFBP-3R with the heptad repeat pattern characteristic of leucine zipper interaction domains identified in erythropoietin receptor and discoidin domain receptor. The *letters in bold* correspond to *a*- and *d*-type interfacial residues in leucine zipper interaction domains. *Right panel*, detection of endogenous IGFBP-3R and adenoviral transduced IGFBP-3R^F by immunoblotting is shown. The IGFBP-3R antibody recognized a 32-kDa species from MDA231 breast cancer cell lysates. *C*, IGFBP-3-IGFBP-3R interaction on cell surface is shown. Monolayer affinity binding data showed a significant increase in radiolabeled IGFBP-3 cell surface binding on cells overexpressing IGFBP-3R compared with control-transfected cells (*left panel*). Competitive inhibition of IGFBP-3 cell surface binding with unlabeled IGFBP-3 in MCF-7 cells is shown (*right panel*). The presence of the FLAG-tag at the C terminus of the IGFBP-3R sequence had no effect. *Error bars* show S.D. $n = 3$ in duplicate. *, $p < 0.1$; **, $p < 0.05$. *D*, subcellular localization of IGFBP-3R by cell fractionation and confocal microscopy is shown. *Left panel*, endogenous IGFBP-3 was detected in plasma membrane and cytoplasmic fractions in human breast cancer cells. Subcellular fractions were prepared by differential centrifugation. 100 μg of proteins were subjected to Western immunoblot with α-IGFBP-3R antibodies. β3 integrin, α-tubulin, and histone deacetylase (*HDAC*) were used as plasma membrane (*Memb*), cytosol (*Cyto*), and nuclear (*Nuc*) markers, respectively. *Right panel*, both endogenous and overexpressed IGFBP-3R is readily detectable on the cell membrane as well as in perinuclear and cytoplasmic area using IGFBP-3R and FLAG M2 antibodies. Hoechst stain (*blue*) was used to identify nuclei.

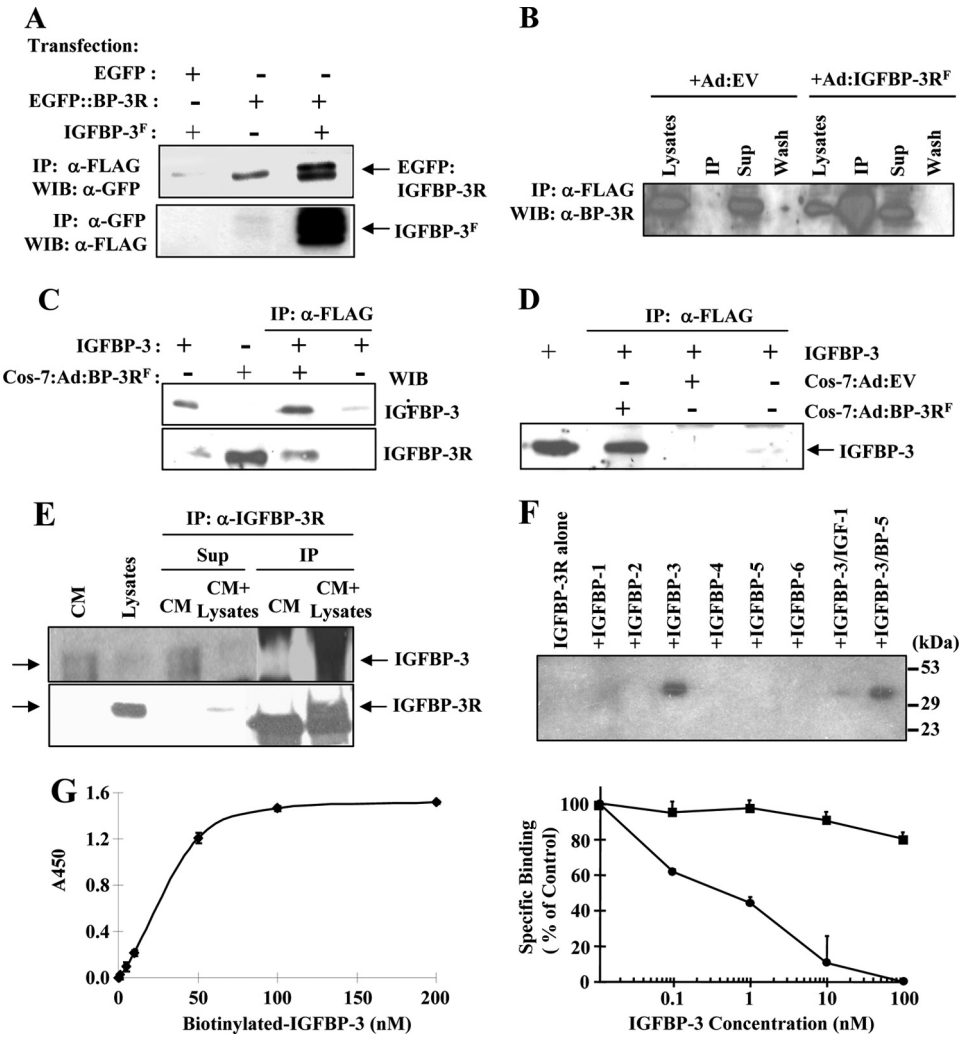

FIGURE 2. **Specific interaction between IGFBP-3 and IGFBP-3R.** *A*, coimmunoprecipitation of IGFBP-3^F and IGFBP-3R fused to EGFP is shown. Cell lysates from transfected cells were immunoprecipitated (*IP*) with either FLAG M2 or GFP antibodies, and immunoprecipitated proteins were detected on Western immunoblots (*WIB*) with the opposing antibody. *B*, detection of endogenous and overexpressed FLAG-tagged IGFBP-3R by IGFBP-3R antibodies is shown. Both endogenous IGFBP-3R and overexpressed IGFBP-3R^F were detected in both cell lysates, whereas FLAG-tagged IGFBP-3R was detected in cell lysates from Ad:IGFBP-3R^F-infected cells after immunoprecipitation with FLAG M2 antibodies. *C*, coimmunoprecipitation of recombinant IGFBP-3 and IGFBP-3R^F is shown. Cos-7 cell lysates from Ad:IGFBP-3R^F-infected cells were immunoprecipitated with FLAG M2 antibodies, and immunoprecipitated proteins were detected on Western immunoblots with either IGFBP-3 or IGFBP-3R antibodies. *D*, coimmunoprecipitation of recombinant IGFBP-3 and IGFBP-3R is shown. Cell lysates from Ad:EV- or Ad:IGFBP-3R^F-infected cells were immunoprecipitated with FLAG M2 antibodies in the presence/absence of IGFBP-3. Immunoprecipitated proteins were detected by Western immunoblots with α-IGFBP-3 antibodies. *E*, shown is coimmunoprecipitation of endogenous IGFBP-3 and IGFBP-3R using MDA231-conditioned media (*CM*) and MCF-7 cell lysates as the source of endogenous IGFBP-3 and IGFBP-3R, respectively. Samples were immunoprecipitated with polyclonal α-IGFBP-3R antibodies and subjected to Western immunoblotting using polyclonal α-IGFBP-3 or α-IGFBP-3 antibodies. 40–45-kDa glycosylated endogenous IGFBP-3 was precipitated with endogenously produced IGFBP-3R (*sixth lane*), whereas IGFBP-3 is undetectable in its immunoprecipitation supernatants (*Sup*, *fourth lane*). Endogenous IGFBP-3R was precipitated by α-IGFBP-3R antibodies (*sixth lane*). In contrast, when IGFBP-3-containing conditioned media was immunoprecipitated in the absence of IGFBP-3R-containing lysates, the IGFBP-3 band was detected only in immunoprecipitation supernatants (*third lane*) but not in the immunoprecipitated samples (*fifth lane*). *F*, representative results of coimmunoprecipitation and Western ligand blotting with IGFBP-3R and IGFBPs 1–6 are shown. 5 nM IGFBPs or in combination with 5 nM IGF-I was incubated with cell lysates from IGFBP-3R^F-overexpressed cells and immunoprecipitated with α-FLAG antibodies. Immunoprecipitated IGFBPs were detected by I^{125}-IGF-I/-II ligand blotting. The interaction of IGFBP-3 and IGFBP-3R was evident, but no interaction was detected with other IGFBPs. *G*, *left panel*, a binding assay between biotinylated IGFBP-3 and IGFBP-3R is shown. *Right panel*, competitive binding of biotinylated IGFBP-3 to IGFBP-3R was assessed in the presence of increasing amounts of unlabeled IGFBP-3 (*closed circle*) or IGFBP-5 (*closed square*). *Error bars* represent S.D. $n = 3$ in duplicate.

of tumor angiogenesis (Fig. 3*C*). These findings indicate that overexpression of IGFBP-3R may enhance paracrine/autocrine-derived IGFBP-3-induced tumor suppression, and thus, IGFBP-3/IGFBP-3R axis represents a novel signaling pathway that inhibits tumor growth.

IGFBP-3R Mediates IGFBP-3-induced Growth Inhibition and Apoptosis—To determine whether IGFBP-3R mediates antiproliferative effect of IGFBP-3, the growth inhibitory actions of endogenous IGFBP-3 via IGFBP-3R were initially tested using IGFBP-3-expressing Hs578T and MDA231 human breast cancer cells, PC-3 prostate cancer cells, and NCI-H157 non-small cell lung carcinoma cells. Significant cell growth inhibition was observed in Ad:IGFBP-3R-infected in a m.o.i.-dependent manner but not Ad:EGFP-infected Hs578T cells (Fig. 4*A*). IGFBP-3R overexpression resulted in growth inhibition up to 90% in IGFBP-3-expressing cancer cells, whereas adenoviral vector itself shows no growth inhibition (Table 1). It was further tested whether IGFBP-3R-induced growth inhibition results from induction of apoptosis. Treatment with the pan-caspase inhibitor z-VAD-fmk resulted in a complete abrogation of both etoposide- and IGFBP-3R-induced cell growth inhibition in Hs578T cells, suggesting that the IGFBP-3R might play a role in IGFBP-3-induced apoptosis (Fig. 4*B*). Furthermore, IGFBP-3R overexpression effectively increases caspase-3/-7 activities in IGFBP-3-expressing cancer cells, reaching maximum activity 48 h after infection ($p < 0.01$ in Hs578T and MDA231 cells and $p < 0.05$ in PC-3 and H157 cells). This suggests that IGFBP-3R mediates endogenous IGFBP-3-induced growth inhibition via activation of caspase-dependent cell death signaling (Fig. 4*C*).

To investigate whether IGFBP-3R is required for the growth inhibitory action of IGFBP-3, IGFBP-3-nonexpressing MCF-7, inducible stably transfected MCF-7:IGFBP-3 subline (MCF-7:IGFBP-3 clone #3 (Ref. 19)), and IGFBP-3-expressing MDA231 breast cancer cells were employed (Fig. 3*D*). Induction of IGFBP-3 expression by 15 μM ponasterone A treatment in MCF-7:IGFBP-3 #3 cells resulted in an inhibition of DNA

synthesis by an average of 45% compared with controls in MCF-7 cells (Fig. 4*D*, *left panel*). With additional overexpression of IGFBP-3R in these cells, DNA synthesis was further inhibited by an average of 65%. Overexpression of IGFBP-3R had no significant effect on DNA synthesis in the absence of IGFBP-3 (either wild type MCF-7 or uninduced MCF-7: IGFBP-3 #3 cells). In IGFBP-3-expressing MDA231 cells, overexpression of IGFBP-3R resulted in a 2.5-fold increase of the cell death compared with controls measured by cell death ELISA assays (Fig. 4*D*, *right panel*). When endogenous IGFBP-3

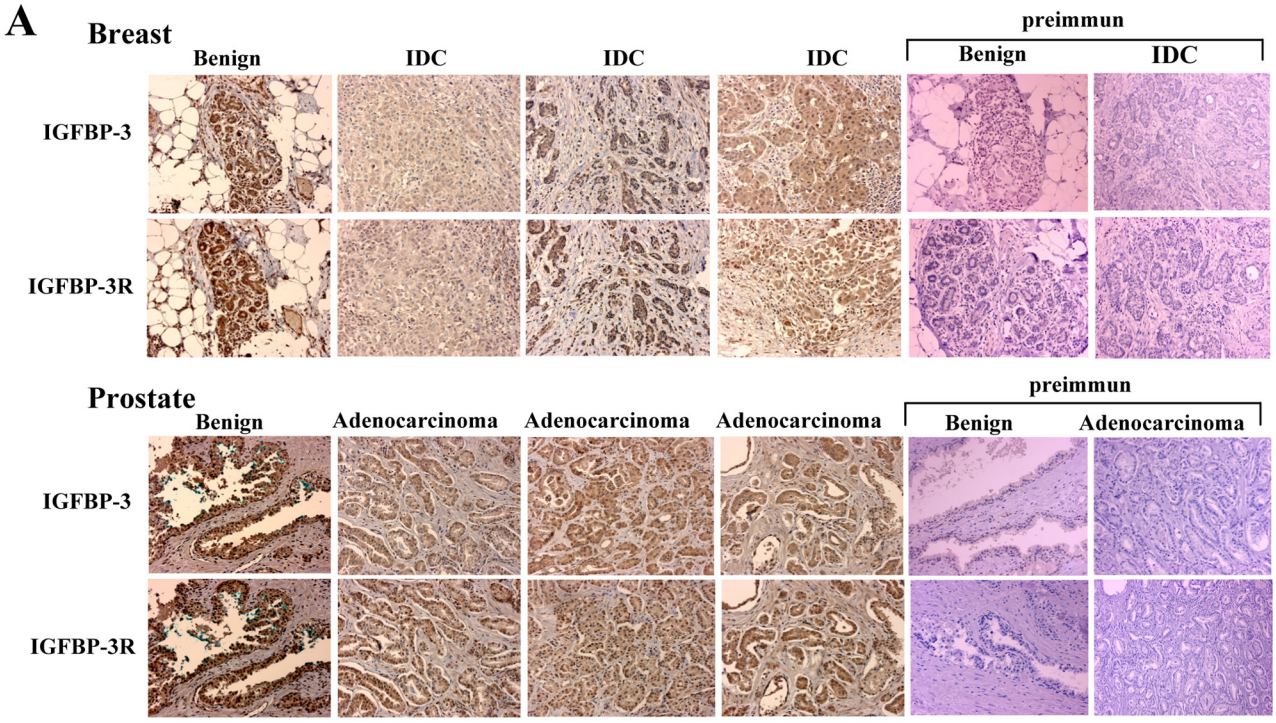

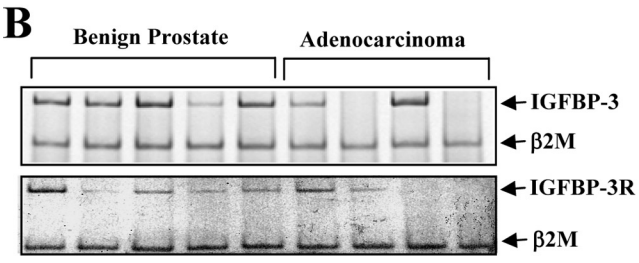

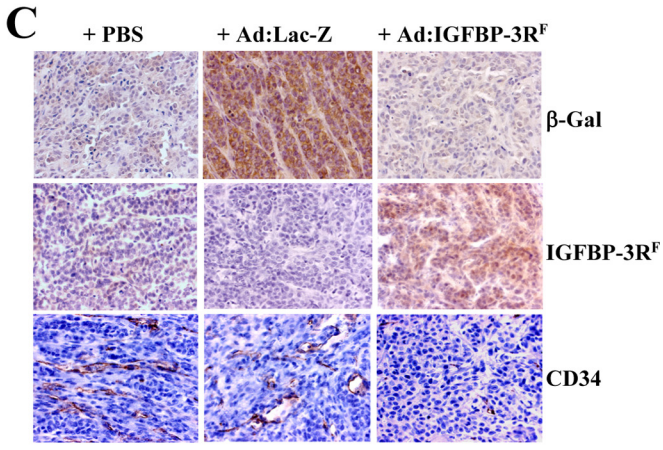

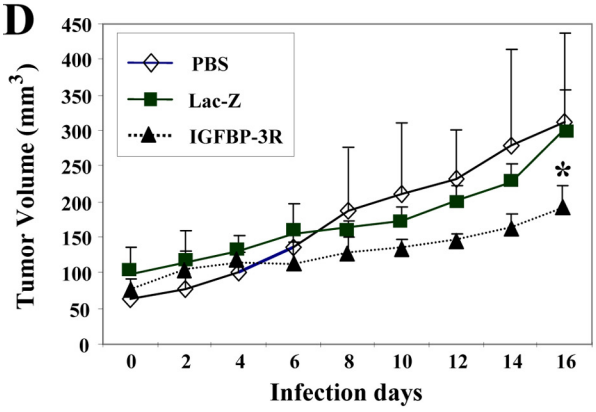

Treatment	*Mean Tumor Volume(mm^3±SD)*	
	Prostate	*Breast*
Control	302 ± 54.5	487 ± 44.0
Ad: IGFBP-3R	193 ± 28.6	280 ±108.1

was suppressed by treatment of IGFBP-3 shRNA (23) in these cells, IGFBP-3R overexpression-induced cell death was significantly inhibited (2.5- *versus* 1.6-fold, $p < 0.05$). Suppression of endogenous IGFBP-3 without IGFBP-3R overexpression shows a slight increase of the cell death up to 1.3-fold.

It was further examined whether IGFBP-3R is required for IGFBP-3-induced apoptosis using IGFBP-3R RNAi techniques in non-IGFBP-3-expressing M12 prostate cancer cells. After verifying a significant knockdown of endogenous IGFBP-3R by IGFBP-3R siRNAs at the mRNA and protein levels, IGFBP-3-induced caspase activity was measured. Although overexpression of IGFBP-3 resulted in a 500% increase of caspase activity, specific knockdown of IGFBP-3R completely inhibited IGFBP-3-induced caspase activities (Fig. 4*E*, *top panel*). No inhibitory effect of IGFBP-3R siRNA on caspase activities was observed in control cells or control adenoviral vector-infected cells. Two target sequences corresponding to siRNAs #1 and #3 were further selected to construct shRNA plasmids. As shown in Fig. 4*E*, *bottom panel*, transfection of two IGFBP-3R shRNAs resulted in complete inhibition of IGFBP-3-induced apoptosis with concomitant suppression of endogenous IGFBP-3R expression in M12 cells. These results indicate that IGFBP-3 induces caspase-dependent apoptosis through IGFBP-3R.

IGFBP-3/IGFBP-3R Activates Caspase-8-dependent Cell Death Signaling—To explore the mechanisms by which the IGFBP-3/IGFBP-3R axis induces apoptosis, the hypothesis was tested that IGFBP-3R might be a novel cell death receptor and activate initiator caspases such as caspase-8 and -10 and the subsequent downstream caspases such as caspase-3 and -7. Because IGFBP-3 has been reported to activate caspase-8 but not caspase-10 in breast cancer cells (19), it was tested whether IGFBP-3R attributes to activation of caspase-8 in IGFBP-3-expressing MDA231 breast cancer cells. IGFBP-3R overexpression resulted in activation of caspase-8 and -3 in a time-dependent manner, as shown by a decrease of procaspase-8 and -3 and concomitant appearance of cleaved active forms of both caspases at 36 h after viral infection (Fig. 5*A*). Co-treatment with pan-caspase inhibitor z-VAD-fmk completely prevented the IGFBP-3R-induced caspase-8 and caspase-3/-7 activities and apoptosis (Fig. 5*B*). At the same time, the caspase-8 specific inhibitor z-IETD-fmk completely abolished the changes in not only caspase-8 but also caspase-3/-7 activities and apoptotic index. We further tested the specific role of caspase-8 in the IGFBP-3/IGFBP-3R axis-induced apoptosis using caspase-8 shRNAs (24). Caspase-8 shRNA treatment resulted in more than 80% suppression of endogenous caspase-8 expression and inhibited IGFBP-3/IGFBP-3R-induced apoptosis up to 60% (Fig. 5*C*). These data clearly demonstrate that caspase-8 is a key initiator caspase involved in the induction of apoptosis by the IGFBP-3/IGFBP-3R axis.

Specific Interaction between IGFBP-3R and Caspase-8—Because IGFBP-3R contains no death domain (DD) sequence, which is a critical sequence to recruit adapter proteins such as FADD and caspase-8 to the activated death receptors, the underlying mechanisms for IGFBP-3R-induced activation of caspase-8 were further investigated. Co-immunoprecipitation studies using IGFBP-3R-overexpressed Cos-7 cell lysates clearly demonstrated that IGFBP-3R binds to caspase-8 without FADD (Fig. 5*D*, *left panel*, *third lane*). Further coimmunoprecipitation experiments were performed to verify interaction between endogenous IGFBP-3R and caspase-8 using Cos-7 cells that produce both proteins. Endogenous caspase-8 but not FADD was co-precipitated with endogenously produced IGFBP-3R in Cos-7 cells when IGFBP-3R antibodies were used for immunoprecipitation (Fig. 5*D*, *right panel*, *fourth lane*), whereas neither caspase-8 nor FADD was detected in the immunoprecipitated samples in the absence of α-IGFBP-3R antibodies (*fifth lane*). Because recent studies demonstrated that membrane proteins containing no DD directly interact with caspase-8 and induce apoptosis (25, 26), the direct binding of IGFBP-3R to caspase-8 was investigated using a eukaryotic *in vitro* TNT. IGFBP-3R and caspase-8 were successfully produced by TNT and were comparable with endogenous proteins expressed in human breast cancer cells. When TNT-derived IGFBP-3R and caspase-8 were incubated and immunoprecipitated with IGFBP-3R antibodies, caspase-8 was coprecipitated with IGFBP-3R (Fig. 5*E*). These data collectively suggest that IGFBP-3R exists as a complex with caspase-8 at the resting stage and IGFBP-3 binding to IGFBP-3R activates procaspase-8 and release from the IGFBP-3R, subsequently activating executioner caspases such as caspase-3 and -7, thereby inducing apoptosis.

DISCUSSION

The IGF/IGF-IR-independent actions of IGFBP-3 have been shown to contribute to the pathophysiology of a variety of human diseases such as cancer, diabetes, ischemia, and Alzheimer disease (10–14, 27–31). There has been intensive investigation toward characterizing molecular and cellular

FIGURE 3. **Significance of the IGFBP-3/IGFBP-3R axis in human cancer.** *A*, shown are representative immunohistochemistry results of IGFBP-3 and IGFBP-3R in human breast and prostate tissues. Intense brown staining of IGFBP-3 and IGFBP-3R is readily detectable in benign breast and prostate epithelial cells as well as stromal fibroblasts. Both IGFBP-3 and IGFBP-3R were significantly reduced in invasive breast ductal carcinoma (*IDC*) and prostate tumor cells. No detectable staining was observed with IgG-purified preimmune serum. Original magnification, 200×. *B*, the expression of IGFBP-3 and IGFBP-3R in normal and malignant prostate specimens was analyzed by semiquantitative RT-PCR. Results were normalized to β_2-microglobulin (*β2M*). *C*, the *in vivo* anti-tumor effect of IGFBP-3R is shown. M12 prostate cancer cells were injected into the dorsal flank of athymic nude mice. Once tumor volume reached ~75 mm^3, 5×10^9 plaque-forming units of Ad:IGFBP-$3R^F$ or Ad:Lac-Z in 50 μl of PBS or 50 μl of PBS alone as a control were intratumorally injected. Representative immunohistochemistry results of M12 cell tumor sample 10-day post-second infection are shown. Intense brown staining of β-galactosidase (*β-gal*) and IGFBP-$3R^F$ were detected in Ad:LacZ- and Ad:IGFBP-3R-infected tumors, respectively. CD34 staining was significantly reduced in Ad:IGFBP-3R-infected tumors. Original magnification, 400×. *D*, decreased size of M12 prostate tumors after adenovirus-mediated IGFBP-3R over-expression is shown. Tumor size and volume were measured every 2 days for 16 days after injection. Results were expressed as the mean (±S.D.) tumor volume ($n = 3$ for each group) relative to the tumor volume at the time of adenovirus injection (day 0). *, $p < 0.01$ (compared with control Ad:Lac-Z infection). Similar results were obtained from MDA231 breast tumor bearing athymic nude mice ($n = 3$ for each group).

mechanisms for IGF/IGF-IR-independent anti-tumor effects of IGFBP-3 in human cancer *in vitro* and *in vivo*. IGFBP-3 appears to exert its IGF/IGF-IR-independent biological actions through interaction with a variety of binding partners on the cell surface and within cells. IGFBP-3 binds to the low density lipoprotein receptor-related protein-1/

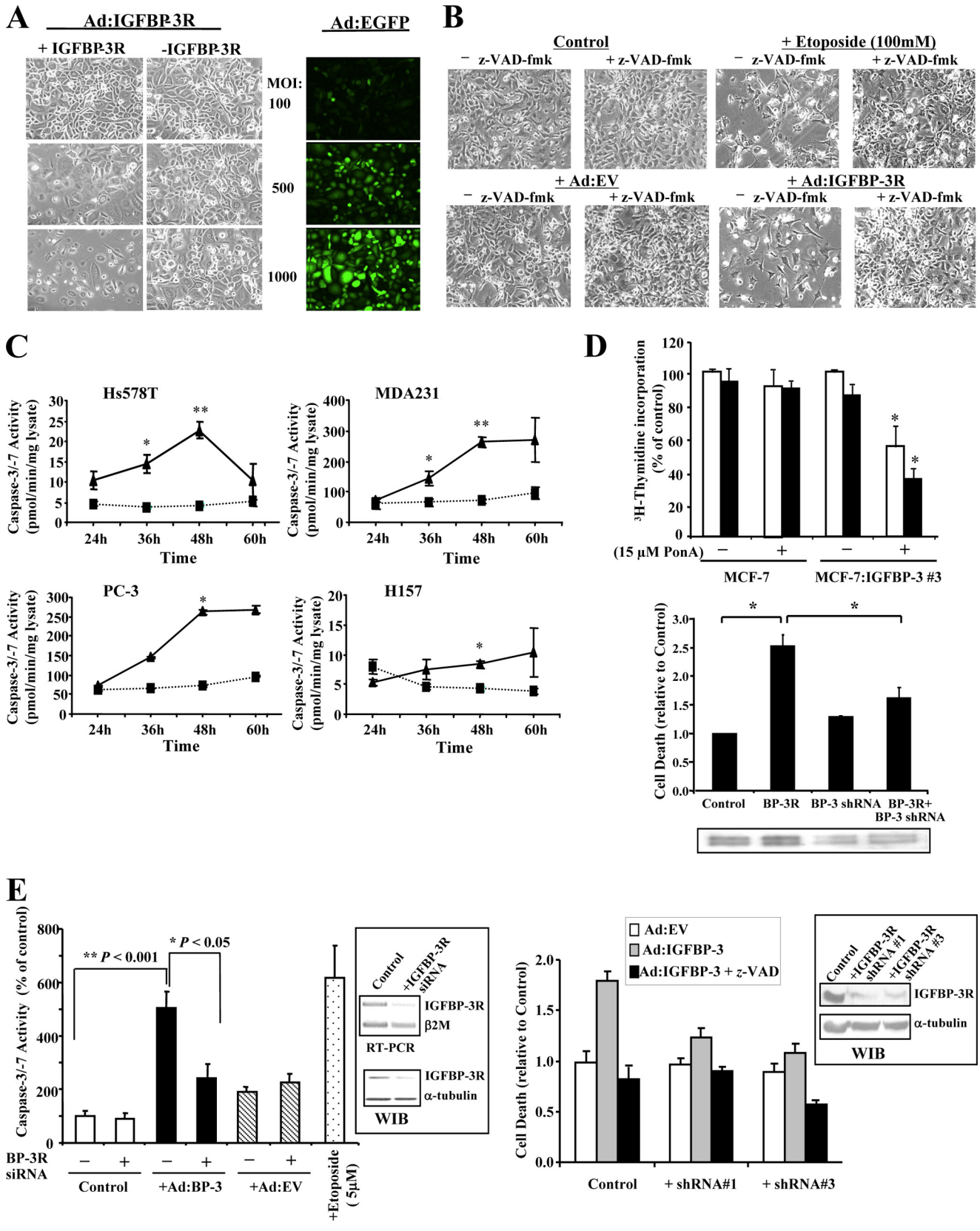

TABLE 1

Anti-proliferative effects of IGFBP-3R

IGFBP-3-expressing human cancer cells were infected with Ad:IGFBP-3R or Ad:EV with and an m.o.i. 500 for Hs578T and an m.o.i. 250 for other cancer cells. MTT assay was performed after 3 days of infection. *Error bars* show S.D. $n = 3$ in triplicate.

Cell lines	A492 reading		Cell growth
	Control	+IGFBP-3R	
	Arbitrary units		*% of control*
Hs578T	1.86 ± 0.16	0.79 ± 0.13	42 ± 2.0[a]
MDA231	0.38 ± 0.18	0.08 ± 0.05	21 ± 4.0[a]
PC-3	0.62 ± 0.13	0.06 ± 0.06	10 ± 2.9[a]
NCI-H157	1.82 ± 0.38	0.53 ± 0.19	29 ± 3.0[a]

[a] $p < 0.001$.

α_2M receptor (15), autocrine motility factor/phosphoglucose isomerase (32), caveolin, and transferrin/transferrin receptor (33, 34) on the cancer cell surface. Functional significance of these binding partners on the IGF/IGF-IR-independent actions of IGFBP-3 is largely unknown, although some studies suggested that these interactions may mediate antiproliferative effects of IGFBP-3 or may result in IGFBP-3 internalization and subsequent biological actions in cytoplasmic and nuclear compartments. In addition, IGFBP-3 is also shown to inhibit cell growth and induce apoptosis through interaction with nuclear proteins such as retinoid X receptor (RXR)-α, retinoic acid receptor (RAR), and Nur77 (35). IGFBP-3 binds RXR-α and RAR and subsequently modulates RAR/RXR and RXR/Nur77 signaling, thereby inducing apoptosis (36, 37). However, recent studies also showed that IGFBP-3 mutants that failed to translocate to the nucleus and lost binding ability to RXR-α still induced apoptosis in breast cancer cells (38, 39). Current findings suggest that IGFBP-3 may utilize multiple mechanisms for its antitumor actions depending upon the cellular environment, or a major key IGFBP-3 signaling pathway is not yet identified.

This is the first report of an authentic IGFBP-3 receptor that interacts and functions cooperatively with IGFBP-3 in its IGF/IGF-IR-independent antiproliferative and proapoptotic functions in cancer cells. Current findings provide evidence for IGFBP-3R as a cell surface receptor for IGFBP-3, including subcellular localization of IGFBP-3R using cell surface binding, cell fractionation, and confocal microscopy, specific interaction of IGFBP-3 with IGFBP-3R on the cell surface, and indispensability of IGFBP-3R for IGFBP-3-induced antiproliferative and proapoptotic functions in cancer cells. Apoptosis can be triggered by internal signals (the intrinsic or mitochondrial pathway) or external signals (the extrinsic or death receptor pathway) (40, 41). The initiator caspase in the mitochondrial pathway is caspase-9, which subsequently activates the executioner caspases -3, -6, and -7. In contrast, the initiator caspase of the death receptor pathway is caspase-8. Caspase-8 (like caspase-9) further activates the cascade of executioner caspases (-3, -6, and -7). Recent studies reported that the growth inhibitory effect of IGFBP-3 results mainly from its induction of apoptosis via activation of caspases-8 and -7 without release of cytochrome *c* into the cytosol and caspase-9 activation in breast cancer cells, suggesting that IGFBP-3 induces apoptosis through the activation of caspases via a death receptor-mediated pathway (19). Hence, IGFBP-3R could be responsible for IGFBP-3-induced activation of the death receptor-mediated pathway. It is noted that IGFBP-3 has also been shown to induce the mitochondria-mediated apoptosis by suppression of antiapoptotic proteins Bcl-2 and Bcl-X_L (42) or interaction with RXR-α and Nur77 (35–37). However, our IGFBP-3R siRNA data clearly demonstrate that IGFBP-3R is required for IGFBP-3-induced caspase-3/-7 activity, and the preceding activation of caspase-8 is indispensable for IGFBP-3-induced apoptosis in our cell systems.

IGFBP-3R possesses very unique characteristics; its putative transmembrane domain contains a leucine zipper-like heptad repeat pattern of amino acids. Only a few proteins such as erythropoietin receptor and discoidin domain receptor are known to possess transmembrane leucine zipper sequences, which may involve dimerization/oligomerization of membrane proteins (21, 22). Interestingly, the transmembrane leucine zipper sequences of IGFBP-3R are similar to those in erythropoietin receptor; in particular, Ser^{203}, Leu^{206}, Ser^{210}, and Leu^{213} in IGFBP-3R are identical to Ser^{231}, Leu^{234}, Ser^{238}, and Leu^{241} that occupy *a* and *d* positions of an $(abcdefg)_n$ heptad repeat motif in transmembrane leucine zipper sequences in erythropoietin receptor (Fig. 1*B*,

FIGURE 4. **IGFBP-3R mediates IGFBP-3-induced growth inhibition and apoptosis.** *A*, growth inhibition by adenoviral-transduced IGFBP-3R is shown. Efficiency of adenoviral infection was visualized under fluorescence microscopy using Ad:EGFP ranging form an m.o.i. of 100 to 1000 in IGFBP-3-expressing Hs578T human breast cancer cells (*right panel*). Significant cell growth inhibition was observed in Ad:IGFBP-3R-infected but not Ad:EGFP-infected IGFBP-3-expressing Hs578T cells after 48 h of infection (*left panel*). *B*, overexpression of IGFBP-3R in Hs578T human breast cancer cells caused significant growth inhibition, but co-treatment with pan-caspase inhibitor z-VAD-fmk abrogated IGFBP-3R-induced growth inhibition. Etoposide was used as a positive control for induction of apoptosis. *C*, overexpression of IGFBP-3R in IGFBP-3-expressing human cancer cells resulted in a significant increase of apoptosis, as measured by a caspase-3/-7 activity assay. ■, +Ad:LacZ; ▲; +Ad:IGFBP-3R. *Error bars* represent S.D. $n = 3$ in triplicate. *, $p < 0.05$; **, $p < 0.001$. *D*, shown is a demonstration of the requirement of IGFBP-3R for IGFBP-3-induced biological functions in IGFBP-3-nonexpressing MCF-7 (*left panel*) and IGFBP-3-expressing MDA231 cells (*right panel*). *Left panel*, MCF-7 and MCF-7:IGFBP-3 #3 cells were infected with Ad:IGFBP-3R (*closed*) or Ad:EV (*open*) with/without 15 μM ponasterone A treatment and subjected to a [^{3}H]thymidine incorporation assay. *Right panel*, IGFBP-3-expressing MDA231 cells were infected with Ad:IGFBP-3R in the presence or absence of IGFBP-3 shRNA retrovirus. The cells were harvested on day 5, and apoptotic cell death was measured by the quantitative detection of histone-associated DNA fragments using the cell death detection ELISA assays. IGFBP-3R overexpression resulted in induction of cell death, but its effects were inhibited by cotreatment with IGFBP-3 shRNA. *Error bars* show S.D. $n = 3$ in triplicate; *, $p < 0.05$. The pSRN-IGFBP-3 shRNA inhibited endogenous IGFBP-3 expression. Conditioned media were collected and subjected to western immunoblots with α-IGFBP-3 antibodies (insert). *E*, shown is suppression of IGFBP-3-induced caspase activity (*top panel*) and apoptosis (*bottom panel*) by IGFBP-3R siRNAs and shRNAs, respectively. *Top panel*, 20 nM IGFBP-3R siRNAs were transfected for 6 days in M12 prostate cancer cells. Total RNA and cell lysates were collected and subjected to RT-PCR and Western immunoblots (*WIB*), respectively (*inset*). M12 cells were infected with Ad:IGFBP-3 (m.o.i. 250) or Ad:EV (m.o.i. 250) in the presence of IGFBP-3R or nonspecific control siRNAs. Cell lysates were collected and subjected to a caspase-3/-7 activity assay. Five μM etoposide was used as a positive control for induction of caspase activity. *Error bars* show S.D. $n = 3$ in duplicate. *, $p < 0.05$; **, $p < 0.001$. *Bottom panel*, M12 cells were transfected with pSRN, pSRN-IGFBP-3R shRNA #1, or pSRN-IGFBP-3R shRNA #3 using Lipofectamine 2000 (Invitrogen) on Day 2 and Day 4 in the presence of 10% FBS. The cells were infected with Ad:IGFBP-3 (m.o.i. 100) or Ad:EV (m.o.i. 100) in the presence of 1% FBS on day 5. The cells were harvested on day 7 and subjected to cell death ELISA assays. Some cells were treated twice with 50 μM pan-caspase inhibitors (z-VAD-fmk) on days 5 and 6. Cell lysates were subjected to Western immunoblots (*inset*).

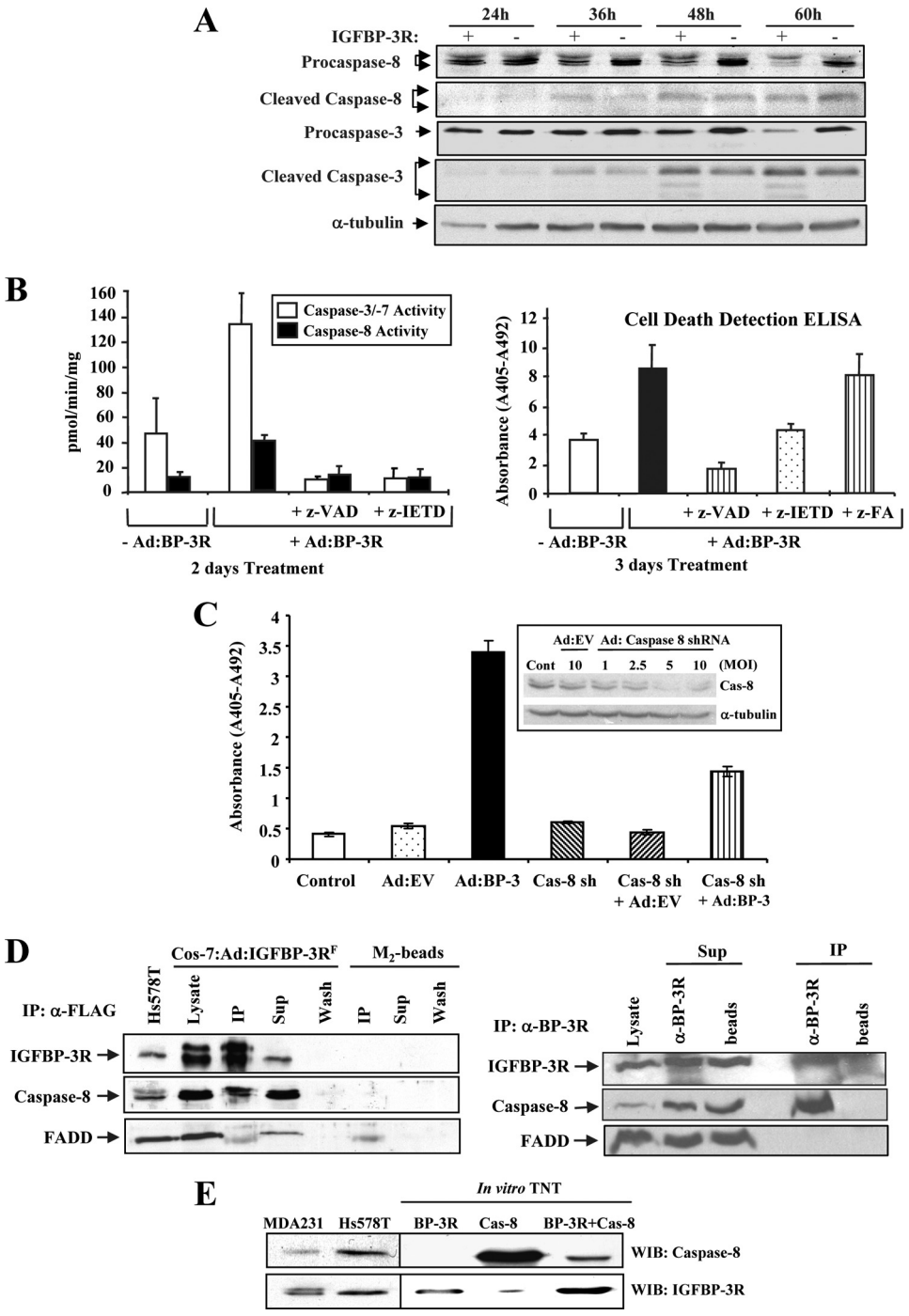

FIGURE 5. **Potential mechanism of IGFBP-3/IGFBP-3R-induced caspase-dependent apoptosis.** *A*, overexpression of IGFBP-3R in IGFBP-3-expressing MDA231 breast cancer cells resulted in activation of caspase-8 and -3 in a time-dependent manner. MDA231 cells were infected with Ad:IGFBP-3R or Ad:EV, and inactive and cleaved active forms of caspase-3 and -8 were detected by immunoblotting. *B*, overexpression of IGFBP-3R in IGFBP-3-expressing MDA231 breast cancer cells resulted in activation of caspase-3/-7 and -8 activities (*left panel*) and apoptosis (*right panel*). IGFBP-3R effects were abolished by cotreatment with pan-caspase and caspase-8 inhibitors (z-VAD-fmk and z-IETD-fmk) but not by inactive caspase inhibitor (z-FA-fmk). *Error bars* show S.D. $n = 3$ in duplicate. *C*, infection of Ad:caspase-8 shRNA inhibited endogenous caspase-8 expression in a m.o.i.-dependent manner (*inset*), and Ad:caspase-8 shRNA (m.o.i. 5) abolished IGFBP-3-induced apoptosis in non-IGFBP-3-expressing T47D breast cancer cells. *Error bars* show S.D. $n = 3$ in duplicate. *Cont*, control. *D*, IGFBP-3R pulled down caspase-8 but not FADD. *Left panel*, IGFBP-3R-overexpressed Cos-7 cell lysates were coimmunoprecipitated (*IP*) with FLAG M2-agarose beads and immunoblotted for IGFBP-3R, caspase-8, and FADD. *Right panel*, coimmunoprecipitation of endogenous IGFBP-3R and caspase-8 is shown. *Sup*, supernatant. Cos-7 cell lysates were immunoprecipitated with polyclonal α-IGFBP-3R antibodies or protein A/G beads alone and subjected to Western immunoblotting using polyclonal α-IGFBP-3R or monoclonal α-caspase-8 or α-FADD antibodies. Endogenous caspase-8 but not FADD was co-precipitated with endogenously produced IGFBP-3R when α-IGFBP-3R antibodies were used for immunoprecipitation (*lane 4*). *E*, a direct binding between IGFBP-3R and caspase-8 is shown. IGFBP-3R (*third lane 3*) and caspase-8 (*fourth lane*) produced by the *in vitro* TNT were comparable with endogenous proteins expressed in MDA-231 and Hs578T breast cancer cells. Coimmunoprecipitation of the mixed samples with α-IGFBP-3R antibodies resulted in pulldown of caspase-8 with IGFBP-3R (*lane 5*). *WIB*, Western immunoblot.

inset). Recent studies demonstrated that those sequences are critical to form the dimer/oligomers in erythropoietin receptor (21). Further structure-function analysis using specific mutants would warrant the significance of the transmembrane leucine zipper sequences on the activity and signaling pathway of the IGFBP-3R. Additionally, IGFBP-3R interacts with initiator caspase-8 without a DD sequence in the intracellular portion of the receptor unlike other known death receptors such as tumor necrosis factor-α (TNF-α) receptor, TNF-related apoptosis-inducing ligand receptor 1 (TRAIL-R1/DR4), TRAIL-R2 (APO-2/DR5), and CD95 (Fas, APO-1). Although the DD sequence is critical in forming death-inducing signaling complex (DISC) by recruiting adaptor proteins (FADD) and initiator caspases (caspase-8) after receptor activation, recent studies demonstrated that clusters of unligated integrins containing no DD directly interact with caspase-8 and induce apoptosis (26). In addition, a novel 600-kDa complex has been shown to recruit and activate caspase-8 independent of FADD and induce apoptosis after p53 activation (25). It is of note that the C-terminal truncated IGFBP-3R mutant shows no interaction with caspase-8, thus strongly suggesting that caspase-8 interacts with the cytoplasmic tail of IGFBP-3R (data not shown). Taken together, we speculate that IGFBP-3R exists as a complex with caspase-8 at the resting stage and IGFBP-3 binding to IGFBP-3R may facilitate dimerization/oligomerization of IGFBP-3R, resulting in proximity-induced activation of the initiator caspase-8 (43).

In summary, we cloned IGFBP-3R, a novel IGFBP-3 death receptor, and identified the IGFBP-3/IGFBP-3R axis as a novel caspase-8-dependent cell death signal in human cancer cells. Our results not only show suppression of IGFBP-3 and/or IGFBP-3R expression in breast and prostate cancer but also the anti-tumor effect of IGFBP-3R *in vivo*. IGFBP-3R represents a new mammalian cell death receptor and promotes the utilization of the IGFBP-3/IGFBP-3R axis for further development of drug screening assays, and diagnostic/prognostic and therapeutic methods for cancer treatment.

Acknowledgments—We gratefully thank Drs. D. G. Stupack (University of California San Diego), D. Mascarenhas (Celtrix Pharmaceuticals), and M. Takaoka for the kind gifts of caspase 8 shRNA, recombinant IGFBP-3, and IGFBP-3 shRNA, respectively. We also thank C. Li (Virginia Commonwealth University) and Drs. P.-H. Hwang and H.-K. G. Yi (Chonbuk National University) for kind assistance.

REFERENCES

1. Firth, S. M., and Baxter, R. C. (2002) *Endocr. Rev.* **23,** 824–854
2. Hwa, V., Oh, Y., and Rosenfeld, R. G. (1999) *Endocr. Rev.* **20,** 761–787
3. Walker, G. E., Kim, H. S., Yang, Y. F., and Oh, Y. (2004) in *Insulin-like Growth Factors* (Le Roith, D., Zumkeller, W., and Baxter, R., eds) pp. 1–22, Landes Bioscience, Austin, TX
4. Zhu, W., Shiojima, I., Ito, Y., Li, Z., Ikeda, H., Yoshida, M., Naito, A. T., Nishi, J., Ueno, H., Umezawa, A., Minamino, T., Nagai, T., Kikuchi, A., Asashima, M., and Komuro, I. (2008) *Nature* **454,** 345–349
5. Perks, C. M., Newcomb, P. V., Norman, M. R., and Holly, J. M. (1999) *J. Mol. Endocrinol.* **22,** 141–150
6. Fu, P., Thompson, J. A., and Bach, L. A. (2007) *J. Biol. Chem.* **282,** 22298–22306
7. Kiepe, D., Van Der Pas, A., Ciarmatori, S., Ständker, L., Schütt, B., Hoeflich, A., Hügel, U., Oh, J., and Tönshoff, B. (2008) *Endocrinology* **149,** 4901–4911
8. Rajaram, S., Baylink, D. J., and Mohan, S. (1997) *Endocr. Rev.* **18,** 801–831
9. Butler, A. A., and Le Roith, D. (2001) *Annu. Rev. Physiol.* **63,** 141–164
10. Oh, Y., Müller, H. L., Lamson, G., and Rosenfeld, R. G. (1993) *J. Biol. Chem.* **268,** 14964–14971
11. Rajah, R., Valentinis, B., and Cohen, P. (1997) *J. Biol. Chem.* **272,** 12181–12188
12. Leal, S. M., Huang, S. S., and Huang, J. S. (1999) *J. Biol. Chem.* **274,** 6711–6717
13. Wu, H. B., Kumar, A., Tsai, W. C., Mascarenhas, D., Healey, J., and Rechler, M. M. (2000) *J. Cell. Biochem.* **77,** 288–297
14. Ikonen, M., Liu, B., Hashimoto, Y., Ma, L., Lee, K. W., Niikura, T., Nishimoto, I., and Cohen, P. (2003) *Proc. Natl. Acad. Sci. U.S.A.* **100,** 13042–13047
15. Huang, S. S., Ling, T. Y., Tseng, W. F., Huang, Y. H., Tang, F. M., Leal, S. M., and Huang, J. S. (2003) *FASEB J.* **17,** 2068–2081
16. Oufattole, M., Lin, S. W., Liu, B., Mascarenhas, D., Cohen, P., and Rodgers, B. D. (2006) *Endocrinology* **147,** 2138–2146
17. Oh, Y., Müller, H. L., Pham, H., and Rosenfeld, R. G. (1993) *J. Biol. Chem.* **268,** 26045–26048
18. Yamanaka, Y., Fowlkes, J. L., Wilson, E. M., Rosenfeld, R. G., and Oh, Y. (1999) *Endocrinology* **140,** 1319–1328
19. Kim, H. S., Ingermann, A. R., Tsubaki, J., Twigg, S. M., Walker, G. E., and Oh, Y. (2004) *Cancer Res.* **64,** 2229–2237
20. Mishra, S., and Murphy, L. J. (2004) *Mol. Cell. Biochem.* **267,** 83–89
21. Ruan, W., Becker, V., Klingmüller, U., and Langosch, D. (2004) *J. Biol. Chem.* **279,** 3273–3279
22. Noordeen, N. A., Carafoli, F., Hohenester, E., Horton, M. A., and Leitinger, B. (2006) *J. Biol. Chem.* **281,** 22744–22751
23. Takaoka, M., Harada, H., Andl, C. D., Oyama, K., Naomoto, Y., Dempsey, K. L., Klein-Szanto, A. J., El-Deiry, W. S., Grimberg, A., and Nakagawa, H. (2004) *Cancer Res.* **64,** 7711–7723
24. Stupack, D. G., Teitz, T., Potter, M. D., Mikolon, D., Houghton, P. J., Kidd, V. J., Lahti, J. M., and Cheresh, D. A. (2006) *Nature* **439,** 95–99
25. Ding, H. F., Lin, Y. L., McGill, G., Juo, P., Zhu, H., Blenis, J., Yuan, J., and Fisher, D. E. (2000) *J. Biol. Chem.* **275,** 38905–38911
26. Zhao, H., Ross, F. P., and Teitelbaum, S. L. (2005) *Mol. Endocrinol.* **19,** 771–780
27. Grimberg, A., Coleman, C. M., Burns, T. F., Himelstein, B. P., Koch, C. J., Cohen, P., and El-Deiry, W. S. (2005) *J. Clin. Endocrinol. Metab.* **90,** 3568–3574
28. Chen, X., and Ferry, R. J. Jr. (2006) *Growth Horm. IGF Res.* **16,** 41–48
29. Chang, K. H., Chan-Ling, T., McFarland, E. L., Afzal, A., Pan, H., Baxter, L. C., Shaw, L. C., Caballero, S., Sengupta, N., Li Calzi, S., Sullivan, S. M., and Grant, M. B. (2007) *Proc. Natl. Acad. Sci. U.S.A.* **104,** 10595–10600
30. Lofqvist, C., Chen, J., Connor, K. M., Smith, A. C., Aderman, C. M., Liu, N., Pintar, J. E., Ludwig, T., Hellstrom, A., and Smith, L. E. (2007) *Proc. Natl. Acad. Sci. U.S.A.* **104,** 10589–10594
31. Williams, A. C., Smartt, H., H.-Zadeh, A. M., Macfarlane, M., Paraskeva, C., and Collard, T. J. (2007) *Cell Death Differ.* **14,** 137–145
32. Mishra, S., Raz, A., and Murphy, L. J. (2004) *Cancer Res.* **64,** 2516–2522
33. Lee, K. W., Liu, B., Ma, L., Li, H., Bang, P., Koeffler, H. P., and Cohen, P. (2004) *J. Biol. Chem.* **279,** 469–476
34. Weinzimer, S. A., Gibson, T. B., Collett-Solberg, P. F., Khare, A., Liu, B., and Cohen, P. (2001) *J. Clin. Endocrinol. Metab.* **86,** 1806–1813
35. Lee, K. W., Ma, L., Yan, X., Liu, B., Zhang, X. K., and Cohen, P. (2005) *J. Biol. Chem.* **280,** 16942–16948
36. Liu, B., Lee, H. Y., Weinzimer, S. A., Powell, D. R., Clifford, J. L., Kurie, J. M., and Cohen, P. (2000) *J. Biol. Chem.* **275,** 33607–33613
37. Schedlich, L. J., O'Han, M. K., Leong, G. M., and Baxter, R. C. (2004)

Biochem. Biophys. Res. Commun. **314,** 83–88
38. Bhattacharyya, N., Pechhold, K., Shahjee, H., Zappala, G., Elbi, C., Raaka, B., Wiench, M., Hong, J., and Rechler, M. M. (2006) *J. Biol. Chem.* **281,** 24588–24601
39. Zappala, G., Elbi, C., Edwards, J., Gorenstein, J., Rechler, M. M., and Bhattacharyya, N. (2008) *Endocrinology* **149,** 1802–1812
40. Fraser, A., and Evan, G. (1996) *Cell* **85,** 781–784
41. Li, J., and Yuan, J. (2008) *Oncogene* **27,** 6194–6206
42. Butt, A. J., Firth, S. M., King, M. A., and Baxter, R. C. (2000) *J. Biol. Chem.* **275,** 39174–39181
43. Salvesen, G. S., and Dixit, V. M. (1999) *Proc. Natl. Acad. Sci. U.S.A.* **96,** 10964–10967